forum acusticum 2026
8-12 September · Graz, Austria

SCATTERING OF CUT-OFF MODES BY IMPEDANCE DISCONTINUITY IN A LINED DUCT

Aymane Chaabaoui[1], Gwenael Gabard[1], Bruno Mangin[2], Jacky Mardjono[2], Vincent Clair[3]

[1] *Laboratoire d'Acoustique de l'Université du Mans, UMR CNRS 6613, Institut d'Acoustique - Graduate School, CNRS, Le Mans Université, France*
[2] *SAFRAN Aircraft Engines, Villaroche, Rond Point René Ravaud - Réau, 77550 Moisy-Cramayel Cedex, France*
[3] *Ecole Centrale de Lyon, CNRS, Universite Claude Bernard Lyon 1, INSA Lyon, LMFA, UMR5509, 69130, Ecully, France*

This paper is a revised version of the authors' submitted manuscript that was peer-reviewed by at least two anonymous reviewers.

Abstract

Sound scattering induced by a duct wall impedance discontinuity located in proximity to a source is investigated. It is illustrated that, when a liner is positioned in a source's near field, evanescent modes can have a significant impact on the transmitted power, especially close to their cut-off frequency. A parametric study is conducted to highlight how evanescent modes located close to the liner modify the in-duct transmitted power. Sensitivity to various parameters such as frequency, source-liner distance, liner length, liner impedance and source modes is investigated. It is demonstrated that, for some configurations, the optimisation of acoustic treatments must take into consideration the near field in order to accurately predict liner performance.

Keywords: *duct, liner, scattering, evanescent modes, impedance discontinuity*

1. Introduction

The increase of the bypass ratio (BPR) of turbofan engines is a well established approach for reducing aircraft engines fuel consumption and therefore emissions. Increasing the BPR leads to bigger nacelles, and shortening the nacelles is a possible solution to avoid an associated mass increase. A consequence is a reduction of acoustically treated areas, which compromises their performance [1]. In addition to being short, liners will be placed in the source's near field. This introduces additional acoustical scattering that may result in a degradation of liner performance.

The acoustic generation as well as the propagation of acoustic waves are modified by the presence of the liner in the proximity of the source. The alteration of sound generation in the presence of a liner is well established in the literature [2]–[4]. As for sound propagation, the transition between a hard wall and a lined wall creates an impedance discontinuity. This results in sound scattering, extensively studied in literature for propagative modes [5]–[11]. In fact, for long nacelles where the liner is far from the acoustic sources, evanescent modes can be neglected at the impedance discontinuity. However, for some future architectures, evanescent modes levels are not as negligible at the impedance discontinuity. There, scattering allows evanescent modes to transfer energy to propagative modes, possibly leading to a significant increase in the transmitted acoustic power. Two types of scattering can occur. When the impedance discontinuity is axial, energy scatters among radial modes of the same azimuthal order, as studied by McAlpine et al. [12] for a single propagative mode. When the impedance discontinuity is azimuthal, as in [13], [14], energy scatters among azimuthal modes. Consequently, Tam et al. [14] recommended moving liner splices far away from the fan because of the energy scattering from evanescent to propagative modes.

In this article, we focus on the propagation of sound in an infinite uniform circular duct carrying a uniform mean flow, for which only the presence of a liner can cause scattering. The impact of the liner on the sound generation is not considered. The source is a single evanescent or propagative mode. The effect of scattering on the transmitted power is investigated as a function of different parameters such as frequency, source-liner distance, liner impedance, liner length, and source radial and azimuthal order.

Corresponding author: *aymane.chaabaoui@safrangroup.com.*

2. Formulation of the problem

We consider sound propagation in a straight circular duct of radius a. The duct is composed of three segments: two rigid walls (left and right) and a lined segment of length L in between, with a locally reacting wall modelled by a surface impedance Z. The duct carries an axial and uniform flow U_0 with density ρ_0 and sound velocity c_0. An acoustic incident field is injected at $x = 0$ and reaches a wall impedance discontinuity at $x = d$ and $x = d + L$. The duct geometry is presented in figure 1. A cylindrical frame (x, r, θ) is used in the following.

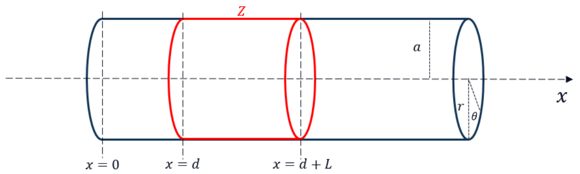

Figure 1: Duct geometry.

2.1. Convected wave equation

The sound propagation is governed by the convected Helmholtz equation with an implicit time dependence $e^{+i\omega t}$, ω being the source pulsation. It is written for the velocity potential ϕ_j in each segment, $j \in [1, 2, 3]$, as

$$\frac{1}{c_0^2}\frac{D_0^2\phi_j}{Dt^2} - \nabla^2\phi_j = 0, \tag{1}$$

where $D_0/Dt = |i\omega + U_0\partial/\partial x|$ is the material derivative. The acoustic pressure perturbation p and velocity perturbation $\mathbf{v}$ can be derived from the velocity potential using

$$p = -\rho_0\left(i\omega + U_0\frac{\partial}{\partial x}\right)\phi \text{ and } \mathbf{v} = \boldsymbol{\nabla}\phi. \tag{2}$$

2.2. Boundary conditions

In a duct, the normal acoustic velocity verifies a boundary condition that depends on the nature of the wall. In the case of a hard wall, the normal acoustic velocity vanishes at the wall $(r = a)$

$$\mathbf{v}\cdot\mathbf{n} = \frac{\partial\phi}{\partial r} = 0, \tag{3}$$

with $\mathbf{n}$ the unit vector normal to the wall surface. In the presence of a flow, the boundary layer modifies the acoustic field acting on the liner. For a uniform axial flow in a straight duct, the Ingard-Myers boundary condition [15] is imposed at $r = a$ for a lined wall:

$$i\omega\frac{\partial\phi}{\partial r} = -\rho_0\left(i\omega + U_0\frac{\partial}{\partial x}\right)^2\left(\frac{\phi}{Z}\right). \tag{4}$$

2.3. Modal decomposition

Since the flow and the boundary conditions do not depend on the axial position, we can write the velocity potential as an infinite sum of modes on each segment j :

$$\phi_j(x, r, \theta, t) = \sum_{m=-\infty}^{\infty}\sum_{n=0}^{\infty}\Big(A^+_{j,mn}\psi^+_{j,mn}(r)e^{-ik^+_{j,mn}x} + A^-_{j,mn}\psi^-_{j,mn}(r)e^{-ik^-_{j,mn}x}\Big)e^{-im\theta}e^{i\omega t}, \tag{5}$$

where m is the azimuthal order and n the radial order. $A^{\pm}_{j,mn}$, $\psi^{\pm}_{j,mn}$, $k^{\pm}_{j,mn}$ are the amplitude, mode radial shape and axial wavenumber respectively of the right-running$(+)$ or left-running$(-)$ mode (m, n) in segment j. The mode shapes ψ_{mn} are normalised in the hard wall segments so that

$$\int_S \psi_{mn}\psi_{pq}\,dS = \delta_{mp}\delta_{nq}.$$

Introducing the reduced axial wavenumber, also called cut-off ratio,

$$\sigma^{\pm}_{j,mn}(\omega) = \pm\sqrt{\omega^2/c_0^2 - (1 - M_0^2)\,\alpha^2_{j,mn}},$$

where $\alpha_{j,mn}$ is the radial wavenumber and $M_0 = U_0/c_0$ is the axial mean flow Mach number, we can write the axial wavenumber $k^{\pm}_{j,mn}$ as

$$k^{\pm}_{j,mn} = \frac{-\omega M_0 + c_0\sigma^{\pm}_{j,mn}}{c_0\,(1 - M_0^2)}.$$

A mode is said to be cut-off if its reduced axial wavenumber σ_{mn} is a pure imaginary number. If σ_{mn} is real, the mode is said to be cut-on. Separating the left-running from the right-running modes in the case of a hard wall is quite direct, modes with a positive σ_{mn} are right-running and those with a negative σ_{mn} are left-running. In the lined segment, it is more complicated and the correct way to separate left-running from right-running modes is still an open question, as we illustrate later.

2.4. Acoustic energy and power

In the case of a hard wall with uniform flow, we can use the orthogonality and normalisation of the modes to write that the total acoustic axial power is [16]

$$\mathcal{P} = \frac{\rho_0\omega}{2}\sum_{m=-\infty}^{\infty}\sum_{n=0}^{\infty}\mathcal{R}e(\sigma^+_{mn})\Big(|A^+_{mn}|^2 - |A^-_{mn}|^2\Big) + 2\mathcal{I}m(\sigma^+_{mn})\mathcal{I}m\left(A^{+*}_{mn}A^-_{mn}\right). \tag{6}$$

For an evanescent mode the associated acoustic power is equal to zero. We may use acoustic energy density as defined by [17], taking the same expression for a single evanescent mode (m, n), the time average of the surface energy density $\mathcal{E}_{mn}$ is

$$\mathcal{E}_{mn} = \frac{\rho_0\,|A_{mn}|^2}{4}\int_S(\alpha^2_{mn} + \frac{m^2}{r^2})\,|\psi_{mn}(r)|^2 + \left|\frac{\partial\psi_{mn}(r)}{\partial r}\right|^2 dS. \tag{7}$$

3. Results

In the following, sound propagation is solved using the same strategy as in [18]. A single right-running mode is imposed at $x = 0$ with unitary amplitude. Modes are then calculated in each segment using a pseudo-spectral method. Finally, mode-matching is applied at each interface to get modal amplitudes in each segment. The left and right segment are semi-infinite, no reflections are considered on both ends of the duct. The injected power $\mathcal{P}_{\text{source}}$, the power in the left segment $(0 < x < d)$ $\mathcal{P}_{\text{left}}$, which is the sum of the power from the injected and the reflected wave, and the power in the right segment $(x > d + L)$ $\mathcal{P}_{\text{right}}$ are defined as :

$$\mathcal{P}_{\text{source}} = \frac{\rho_0\omega}{2} \sum_{m=-\infty}^{\infty} \sum_{n=0}^{\infty} \mathcal{R}e(\sigma^+_{mn}) |A^+_{1,mn}|^2$$

$$\mathcal{P}_{\text{left}} = \frac{\rho_0\omega}{2} \sum_{m=-\infty}^{\infty} \sum_{n=0}^{\infty} \mathcal{R}e(\sigma^+_{mn}) \Big(|A^+_{1,mn}|^2 - |A^-_{1,mn}|^2 \Big) + 2\mathcal{I}m(\sigma^+_{mn}) \mathcal{I}m(A^{+*}_{1,mn} A^-_{1,mn})$$

$$\mathcal{P}_{\text{right}} = \frac{\rho_0\omega}{2} \sum_{m=-\infty}^{\infty} \sum_{n=0}^{\infty} \mathcal{R}e(\sigma^+_{mn}) |A^+_{3,mn}|^2.$$

In the following, distances are scaled by the radius a, velocities by the sound velocity c_0, impedances by $\rho_0 c_0$ and sound frequencies are characterised by the Helmholtz number $He = \omega a / c_0$. The value of the different parameters are chosen to be representative of those in a high BPR turbofan engine. A mode $(m = 1, n = 4)$ is injected at different frequencies around its cut-off frequency He_c :$-0.5 < He - He_c < 0.5$. The flow Mach number is $M_0 = -0.3$ and the liner is located at $d = 0.125$, with a length of $L = 0.25$ and its impedance is set to $Z = 0.2 - \mathrm{i}$. This set of values will be referred to as the reference case. The different powers as a function of Helmholtz number for the reference case are presented in figure 2. In Fig.

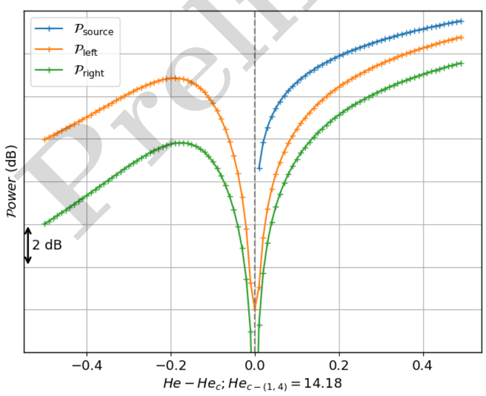

Figure 2: Evolution of the acoustic powers for varying Helmholtz number for the reference case.

2, the behaviour of propagative modes is classical: the injected power is partially reflected and attenuated by the liner. Below cutoff, the injected power is zero, since evanescent modes do not transport energy. However, the interaction between the incident and reflected evanescent waves generates a positive power in the left segment directed towards the liner, where part of it is absorbed and part transmitted. Energy is scattered from the evanescent mode $(m = 1, n = 4)$ to the propagative lower-order modes $(m = 1, n = (0; 1; 2; 3))$.

3.1. Model validation

When solving the eigenvalue problem with the spectral method as in [18], we should distinguish the left-running from the right-running modes. A good criterion used in literature [19] is to draw a diagonal in the complex plane of axial wavenumber. The modes below the diagonal are right-running, and those above are left-running. This criterion works well with hard wall modes. When using the Ingard-Myers boundary condition (eq (4)), surface waves described by [20], [21] appear as acoustic modes but behave differently. Of particular interest are the hydrodynamic instabilities that can appear as left- or right-running acoustic modes growing exponentially in their direction of propagation. Depending on how we interpret these hydrodynamic instabilities, results are significantly different. We present in figure 3 multiple calculations for the reference case: a first calculation using a finite-element code [22], this is useful for validation since no assumptions are made on the modes. Then a mode matching calculation without particular handling of the hydrodynamic instabilities ('no criteria'), with removing the hydrodynamic instabilities ('remove modes'), and with changing the direction of propagation of the hydrodynamic instabilities ('change direction'). In figure 3, it appears that interpreting a hydrodynamic instability as an acoustic mode without particular handling using only the criterion used in [19] misrepresents the acoustic field. Removing these modes from the solution, as was done in [12] and [1] allows for a more reasonable result, but the power is not conserved in the duct. Another idea is to interpret them as modes propagating in the opposite direction, as was done in [23]. Changing the direction of the unstable modes gives the most accurate result, and the acoustic power is conserved and continuous throughout the duct. This is the criterion implemented in the following.

3.2. Parametric study

The purpose of this parametric study is to evaluate the effects of the different parameters on the transmitted power.

3.2.1. Influence of the source-liner distance

First, we look at the effect of the distance between the source and the liner. In figure 4, all parameters are set to their reference values, and we compute the transmitted power on the right segment for different values of source-liner distance d. In figure 4, we can see that the closer the liner is to the source, the more

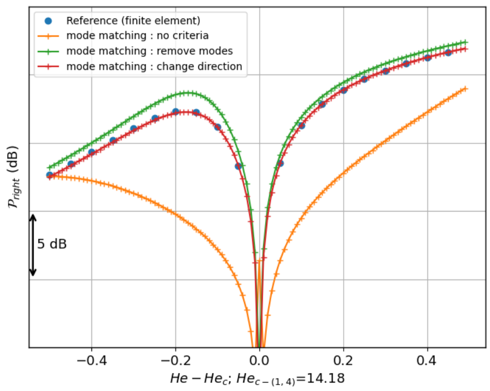

Figure 3: Comparison of transmitted power for different hydrodynamic modes handling for the reference case.

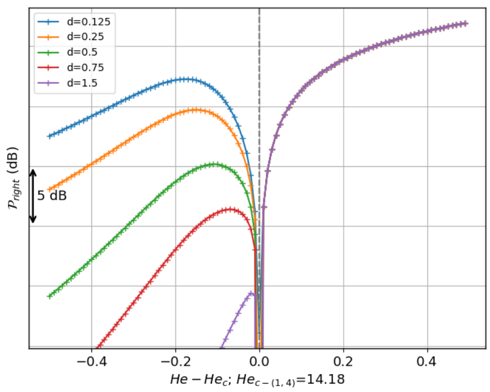

Figure 4: Transmitted power as a function of Helmholtz number for different source-liner distances.

power is transmitted. This is quite easily predictable, the closer the liner is to the source the more energetic are the evanescent modes when they reach the impedance discontinuity, which means that more energy is scattered to propagative modes. The power is proportional to the distance between the source and the liner as $\mathcal{P}_{\text{right}}(d) \propto \left(\mathrm{e}^{-k_{mn}d}\right)^2$. For the reference configuration $d = 0.125$, we can also see in figure 4 that the transmitted power is of the same order of magnitude close to the cut-off frequency, whether the mode is cut-off or cut-on. This highlights the importance of evanescent mode relative to propagative modes when the liner is close to the source.

3.2.2. Influence of the impedance

In this part, the effects of the impedance are investigated. The frequency is set to $He - He_c = -0.1$, all other parameters are set to their reference values. In figure 5, the transmitted power is computed for different values of impedance and plotted in the Z-complex plane. In figure 5, we illustrate some trends. Liners with higher resistance ($\mathcal{R}e(Z)$) have a lower percentage of open area [24] and are closer to a hard wall.

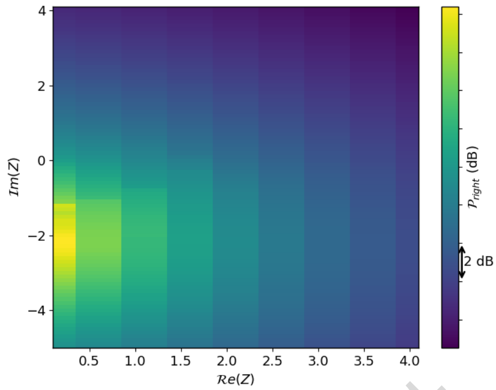

Figure 5: Transmitted power in the Z-complex plane at $He - He_c = -0.1$ for reference configuration.

This results in less scattering and a transmitted power that tends to zero, since only an evanescent mode is injected in the duct. For the same value of resistance, significant differences on the transmitted power are observed depending on the reactance ($\mathcal{I}m(Z)$). This is particularly relevant for liners with low resistance, a difference of up to 10 dB is observed between a reactance value of $\mathcal{I}m(Z) = 2$ and $\mathcal{I}m(Z) = -2$. Plotting the transmitted power in the Z-complex plane when varying the other parameters shows that the global trends are conserved: a maximum value located at a region with lower resistances and positive or negative reactances depending on the distance to cut-off frequency. The value of impedance at which the maximum of transmitted power occurs depends on the liner length, frequency and Mach number. This behaviour is consistent with the mechanism described by Xiong et al. for a rectangular duct in the absence of flow [25]. The observed maximum could result from an excitation of a Fano resonance by the means of a quasi-trapped mode with constructive interferences in the lined region. This resonance is attenuated when the resistance of the liner is increased.

3.2.3. Influence of the mode order

We may now investigate the effects of the mode azimuthal and radial order. Injecting different modes with unitary amplitude does not guarantee that the same energy is injected in the system, in fact higher order evanescent modes are more energetic for the same modal amplitude. Therefore, we need to define a transmission coefficient to take into account the fact that energy levels are different from a mode to another for the same modal amplitude. In order to define a transmission coefficient, the insertion loss has usually been defined in the literature [12], [14], [26]. With evanescent modes, the incident power is equal to zero. In order to define a transmission coefficient, it may be possible to use the reactive part of the incident power (imaginary part), but it tends to zero when the frequency gets closer to cut-off. We can use the power on the left segment as was used by [14], but this will depend on the reflection on the liner. In the following, we suggest using the energy associated to an evanescent mode $\mathcal{E}_{mn}$ defined in equation (7). We define the transmission coefficient β as

$$\beta = 10\log_{10}\left(\frac{\mathcal{P}_t}{\mathcal{E}_{mn}}\right).$$

By comparing β for different mode orders, we ensure that the transmitted power is compared for the same amount of energy injected into the duct. All parameters are set to their reference values, the source is now modified to explore the effects of the order of the mode. In figure 6, the transmission coefficient β is computed at a frequency $He - He_{c,mn} = -0.1$ to guarantee the same "distance" from cut-off for the different modes. Note that only scattering between

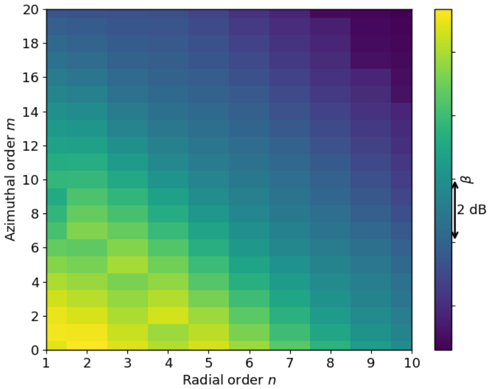

Figure 6: Transmission coefficient for different source modes at $He - He_{c,mn} = -0.1$ for reference configuration.

radial modes is possible, since the discontinuity is only axial. We can see in figure 6 that low order evanescent modes tends to scatter more energy. This may be explained by the fact that for higher azimuthal order, more energy is concentrated near the duct wall [27], [28], which favours energy absorption by the liner. Moreover, higher radial order modes are less sensitive to the impedance discontinuity at the wall because energy is concentrated close to the duct axis, therefore less scattering occurs, which leads to less transmitted power.

3.2.4. Influence of liner length

Following the same methodology, we investigate the influence of the liner's length. In figure 7, all parameters are set to their reference value, and we compute the transmitted power for different liner lengths and different frequencies. As we can see in figure 7, for a cut-on mode, increasing the liner length increases its efficiency. This is not the case for an evanescent mode. In order to try to understand the dependence of the transmitted power on the liner's length, the frequency is fixed at $He - He_c = -0.1$ and the transmission coefficient for different liner lengths and different modes

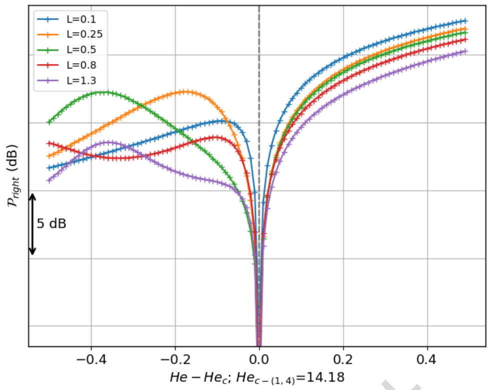

Figure 7: Transmitted power as a function of Helmholtz number for different liner lengths.

is computed to obtain figure 8. Figure 8 shows the

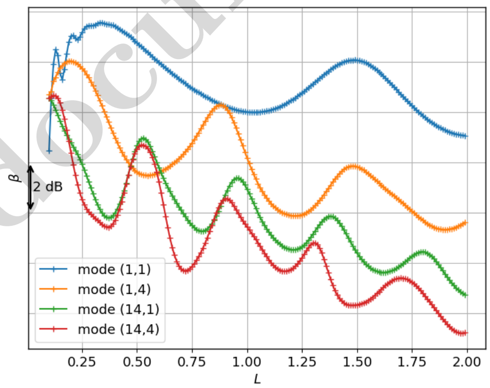

Figure 8: Transmission coefficient as a function of liner length at $He - He_c = -0.1$ for different modes.

existence of local extrema of transmitted power at specific liner lengths. This behaviour may change if the impedance changes, also following the same mechanism as in [25].

4. Conclusion

In this paper, we explored the sensitivity of scattering of cut-off modes to different parameters. A parametric study was performed to demonstrate that evanescent modes have a significant effect when a liner is close to the source. The results indicate that scattering is enhanced for some specific combinations of liner length, frequency, impedance and flow Mach number, which may be associated with an excitation of a Fano resonance in the lined segment. Additionally, it was shown that lower order evanescent modes scatter more energy than higher order ones. This is a preliminary work to understand and quantify the effects of evanescent modes and lay the groundwork to include evanescent modes in the liner optimisation process in the context of turbofan engines.

References

[1] S. Palleja Cabre, "Fan proximity acoustic treatments for improved noise suppression in turbofan engines," Ph.D. dissertation, University of Southampton, 2021.

[2] S. W. Rienstra and B. J. Tester, "An analytic green's function for a lined circular duct containing uniform mean flow," *Journal of Sound and Vibration*, vol. 317, no. 3-5, pp. 994–1016, 2008.

[3] E. Brambley and G. Gabard, "Reflection of an acoustic line source by an impedance surface with uniform flow," *Journal of Sound and Vibration*, vol. 333, no. 21, pp. 5548–5565, 2014.

[4] S. Palleja-Cabre, B. J. Tester, and R. J. Astley, "Modelling of ducted noise sources in the proximity of acoustic liners," *Journal of Sound and Vibration*, vol. 517, p. 116 548, 2022.

[5] D. Lansing and W. Zorumski, "Effects of wall admittance changes on duct transmission and radiation of sound," *Journal of Sound and Vibration*, vol. 27, no. 1, pp. 85–100, 1973.

[6] J. Unruh, "Finite length tuning for low frequency lining design," *Journal of Sound and Vibration*, vol. 45, no. 1, pp. 5–14, 1976.

[7] K. J. Baumeister, "Evaluation of optimized multisectioned acoustic liners," *AIAA Journal*, vol. 17, no. 11, pp. 1185–1192, 1979.

[8] W. Koch and W. Mohring, "Eigensolutions for liners in uniform mean flow ducts," *AIAA Journal*, vol. 21, no. 2, pp. 200–213, 1983.

[9] S. Rienstra and N. Peake, "Modal scattering at an impedance transition in a lined flow duct," in *11th AIAA/CEAS Aeroacoustics Conference*, 2005, p. 2852.

[10] S. W. Rienstra, "Acoustic scattering at a hard–soft lining transition in a flow duct," *Journal of Engineering Mathematics*, vol. 59, no. 4, pp. 451–475, 2007.

[11] B. Mangin, M. Daroukh, and G. Gabard, "Propagation of acoustic waves in ducts with flow using the multimodal formulation," *AIAA Journal*, vol. 61, no. 6, pp. 2721–2733, 2023.

[12] A. McAlpine, R. J. Astley, V. Hii, N. Baker, and A. Kempton, "Acoustic scattering by an axially-segmented turbofan inlet duct liner at supersonic fan speeds," *Journal of Sound and Vibration*, vol. 294, no. 4-5, pp. 780–806, 2006.

[13] A. McAlpine and M. Wright, "Acoustic scattering by a spliced turbofan inlet duct liner at supersonic fan speeds," *Journal of Sound and Vibration*, vol. 292, no. 3-5, pp. 911–934, 2006.

[14] C. K. Tam, H. Ju, and E. W. Chien, "Scattering of acoustic duct modes by axial liner splices," *Journal of Sound and Vibration*, vol. 310, no. 4-5, pp. 1014–1035, 2008.

[15] M. Myers, "On the acoustic boundary condition in the presence of flow," *Journal of Sound and vibration*, vol. 71, no. 3, pp. 429–434, 1980.

[16] G. Gabard and R. Astley, "A computational mode-matching approach for sound propagation in three-dimensional ducts with flow," *Journal of Sound and Vibration*, vol. 315, no. 4-5, pp. 1103–1124, 2008.

[17] C. Morfey, "Acoustic energy in non-uniform flows," *Journal of Sound and Vibration*, vol. 14, no. 2, pp. 159–170, 1971.

[18] G. Gabard, "Mode-matching techniques for sound propagation in lined ducts with flow," in *16th AIAA/CEAS Aeroacoustics Conference*, 2010, p. 3940.

[19] J. Yang, T. Humbert, J. Golliard, and G. Gabard, "Shear flow effects in a 2d duct: Influence on wave propagation and direct impedance eduction," *Journal of Sound and Vibration*, vol. 576, p. 118 296, 2024.

[20] S. W. Rienstra, "A classification of duct modes based on surface waves," *Wave motion*, vol. 37, no. 2, pp. 119–135, 2003.

[21] E. J. Brambley and N. Peake, "Classification of aeroacoustically relevant surface modes in cylindrical lined ducts," *Wave motion*, vol. 43, no. 4, pp. 301–310, 2006.

[22] G. Gabard, *GwenaelGabard/pfe*, Nov. 29, 2025. [Online]. Available: `https://github.com/GwenaelGabard/pfe` (visited on 02/20/2026).

[23] S. W. Rienstra, "Fundamentals of duct acoustics," *Von Karman Institute Lecture Notes*, vol. 598, 2015.

[24] R. Motsinger and R. Kraft, *Design and performance of duct acoustic treatment, aeroacoustics of flight vehicles: Theory and practice*, 1995.

[25] L. Xiong, W. Bi, and Y. Aurégan, "Fano resonance scatterings in waveguides with impedance boundary conditions," *The Journal of the Acoustical Society of America*, vol. 139, no. 2, pp. 764–772, 2016.

[26] R. Astley, R. Sugimoto, and P. Mustafi, "Computational aero-acoustics for fan duct propagation and radiation. current status and application to turbofan liner optimisation," *Journal of Sound and Vibration*, vol. 330, no. 16, pp. 3832–3845, 2011.

[27] C. Chapman, "Sound radiation from a cylindrical duct. part 1. ray structure of the duct modes and of the external field," *Journal of Fluid Mechanics*, vol. 281, pp. 293–311, 1994.

[28] F. W. J. Olver, L. C. Maximon, D. Lozier, R. Boisvert, and C. Clark, "Bessel functions," *NIST handbook of mathematical functions*, no. 2655350, pp. 215–286, 2009.